Available online at www.sciencedirect.com
SCIENCE DIRECT®
Bioorganic & Medicinal Chemistry 12 (2004) 4159–4167
Bioorganic & Medicinal Chemistry

Structure–activity relationships of *seco*-prezizaane and picrotoxane/picrodendrane terpenoids by *Quasar* receptor-surface modeling

Thomas J. Schmidt,[a,*] Marion Gurrath[b] and Yoshihisa Ozoe[c]

[a]*Institut für Pharmazeutische Biologie der Heinrich-Heine-Universität Düsseldorf, Universitätsstrasse 1, D-40225 Düsseldorf, Germany*
[b]*Institut für Pharmazeutische Chemie der Heinrich-Heine-Universität Düsseldorf, Universitätsstrasse 1, D-40225 Düsseldorf, Germany*
[c]*Department of Life Science and Biotechnology, Faculty of Life and Environmental Science, Shimane University, Matsue, Shimane 690-8504, Japan*

Received 2 March 2004; revised 12 May 2004; accepted 17 May 2004
Available online 24 June 2004

This work is dedicated to H. M. Schmidt, the first person to isolate anisatin and pseudoanisatin from a North American *Illicium* species,[6] on the occasion of her 40th birthday

Abstract—The *seco*-prezizaane-type sesquiterpenes pseudoanisatin and parviflorolide from *Illicium* are noncompetitive antagonists at housefly (*Musca domestica*) γ-aminobutyric acid (GABA) receptors. They show selectivity toward the insect receptor and thus represent new leads toward selective insecticides. Based on the binding data for 13 *seco*-prezizaane terpenoids and 17 picrotoxane and picrodendrane-type terpenoids to housefly and rat GABA receptors, a QSAR study was conducted by quasi-atomistic receptor-surface modeling (*Quasar*). The resulting models provide insight into the structural basis of selectivity and properties of the binding sites at GABA receptor-coupled chloride channels of insects and mammals.

1. Introduction

γ-Aminobutyric acid (GABA) is a major inhibitory neurotransmitter in both vertebrates and invertebrates. In vertebrates, two major types of GABA receptors are known, ionotropic and G protein-coupled (GPCR) receptors, both important for regulation within the central nervous system.[1] The former receptors are hetero-pentameric ligand-gated chloride channels, where binding of GABA induces the opening of the channels and increased membrane conductance for chloride ions, resulting in hyperpolarization and thereby increasing the potential difference necessary to generate an action potential.[2] In insects, the GABA receptor-coupled chloride channel complex is similar to but pharmacologically distinct from that of mammals. Here, GABA receptors have regulatory function not only in the central but also in the peripheral nervous system.[3,4] Hence, insect GABA receptors are a promising target for insecticides such as fipronil, which acts as a noncompetitive antagonist selectively on insect ionotropic GABA receptors.[5]

A variety of terpenoids of plant origin, such as anisatin **1**, picrotoxinin **14** and several picrodendrins (**18**–**30**), are known to be noncompetitive antagonists of GABA receptors. Anisatin is a poisonous sesquiterpene of the *seco*-prezizaane type isolated from several star anise (*Illicium*) species.[6]

It was recently reported that two other *Illicium*-sesquiterpenes, pseudoanisatin **4** and parviflorolide **5**, possessing the same basic carbon skeleton as **1**, but differing in the mode of substitution and cyclization from the typical convulsant, are selective antagonists toward the insect GABA receptor.[7] The IC_{50} value determined for **4** with respect to specific [^{3}H]EBOB binding to housefly (*Musca domestica*) head membranes was almost as low as that of anisatin while it did not show significant activity toward a preparation from rat brain (*Rattus norvegicus*).[7] The compound furthermore was shown to be toxic to cockroach (*Blattella germanica*) in vivo,[7]

Keywords: GABA antagonists; Terpenoids; Neurotoxins; Insecticides; QSAR.
* Corresponding author. Tel.: +49-211-8114179; fax: +49-211-81119-23; e-mail: schmidtt@uni-duesseldorf.de

0968-0896/$ - see front matter © 2004 Elsevier Ltd. All rights reserved.
doi:10.1016/j.bmc.2004.05.019

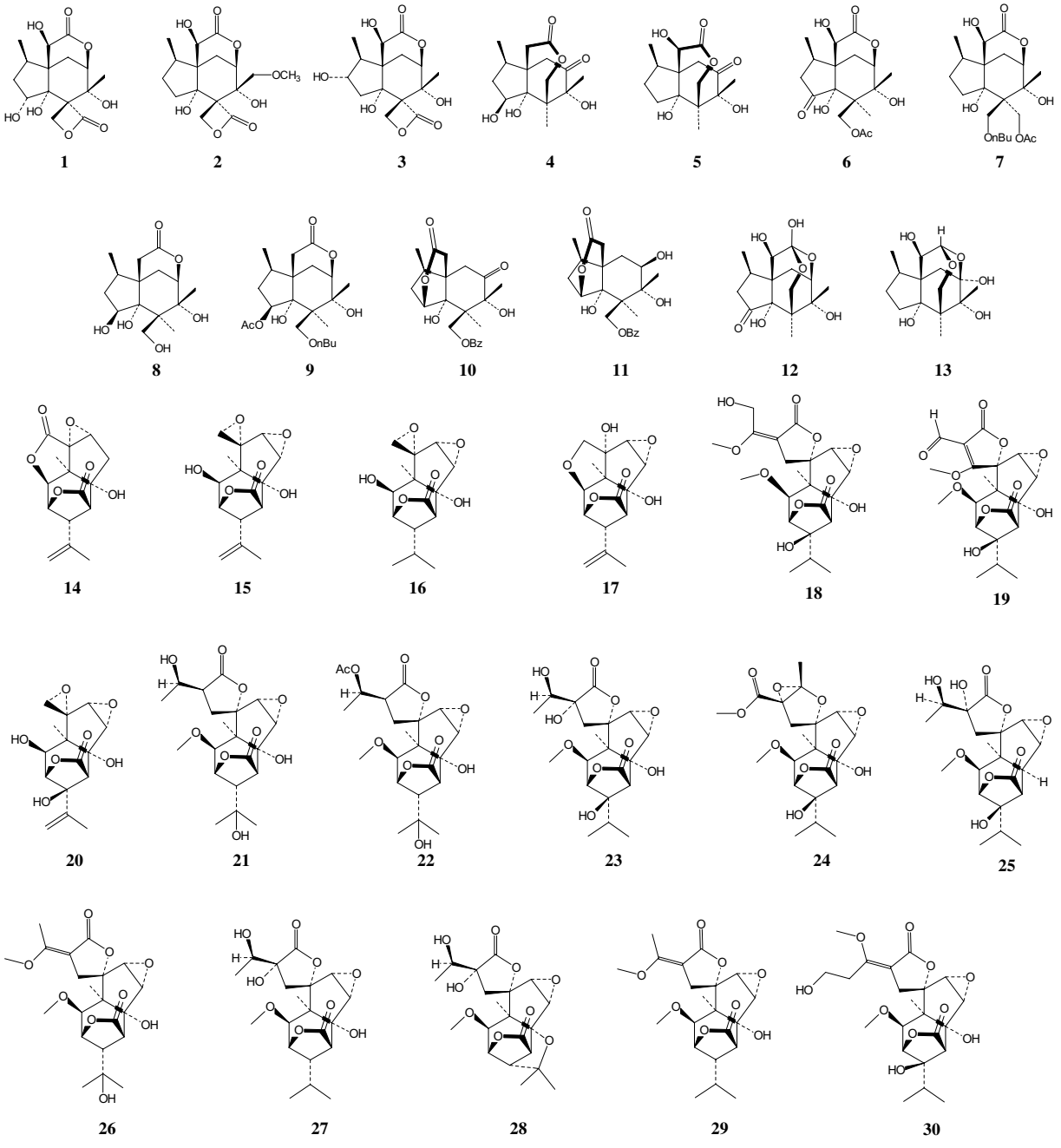

Structures of the *seco*-prezizaane (**1–13**) and picrotoxane/picrodendrane derivatives (**14–30**)

while it had previously been found to be nontoxic to mice at 50 mg/kg.[8]

It was previously demonstrated that *seco*-prezizaane and picrotoxane/picrodendrane-type compounds in spite of their different carbon skeleton are likely to act on GABA receptors by binding to a common binding site.[7] In a similar way as shown for *seco*-prezizaanes, also picrotoxanes/picrodendranes were investigated with respect to differential activity toward insect and mammalian GABA receptors.[9] Also in this case some compounds were shown to act preferentially on the insect receptor. It has long been known that the GABA receptor chloride channel complex in insects and mammals differs in structure[3,4] so that differential binding affinities of antagonists to these receptors could probably be rationalized through differences in protein structure. However, since no information about the three-dimensional structure exists for any of these proteins, direct comparison of 'real' (i.e., atomistic) binding sites and evaluation with respect to structure–activity or structure–selectivity relationships is not possible.

The aim of this study was therefore to shed light on the structural differences between the binding sites for the mentioned classes of terpenoids at insect and mammalian GABA receptors, and on the structural basis of

Table 1. Binding energies of compounds **1**–**30** at the housefly and rat convulsant binding sites (ΔG^0 [kcal/mol] at $T = 298$ K) as obtained from their IC_{50} or %10 μM data measured by displacement of [^{3}H]EBOB from the respective receptors[7,9] and values predicted by the pseudoreceptor models

Compds	Fly		Rat	
	ΔG^0	Pred.	ΔG^0	Pred.
1 Anisatin	**−9.422**	**−8.912**	**−8.955**	**−7.586**
2 Veranisatin A	**−9.684**	−9.772	−8.931	−8.543
3 2α-Hydroxyneoanisatin	−7.071	−7.488	−5.157*	−5.966
4 Pseudoanisatin	−8.761	−8.497	−5.133*	−4.823
5 Parviflorolide	**−8.670**	**−9.245**	**−5.204***	**−6.707**
6 d374	−7.686	−7.089	−5.081*	−4.352
7 d355510	−7.431	−7.382	−4.091*	−4.255
8 d425	**−6.962**	**−6.951**	−3.409*	−3.650
9 d35557	−5.602*	−5.733	−4.363*	−4.420
10 d410	**−6.463***	**−6.716**	**−5.351***	**−4.719**
11 Dunnianin	−5.549*	−5.713	−5.069*	−5.237
12 d4214	−6.032*	−5.886	−5.050*	−4.915
13 Cycloparvifloralone	−6.168*	−6.254	−5.093*	−5.329
14 Picrotoxinin	−9.601	−9.371	−8.464	−8.310
15 Tutin	−8.681	−8.340	−8.212	−7.296
16 Dihydrotutin	**−8.436**	**−8.847**	**−7.291**	**−8.084**
17 Corianin	−8.838	−8.664	−5.962	−6.662
18 Picrodendrin A	−8.401	−8.749	−8.957*	−9.067
19 Picrodendrin B	−8.803	−8.379	−6.662	−6.007
20 Picrodendrin C	−6.710	−7.099	−6.042	−6.134
21 Picrodendrin E	−8.187	−8.418	−5.526*	−5.777
22 Picrodendrin E-18-Ac	−6.662	−6.671	−5.089*	−5.433
23 Picrodendrin F	−7.511	−7.959	−4.363*	−5.389
24 Picrodendrin G	−7.375	−7.962	−4.636*	−5.090
25 Picrodendrin L	−7.439	−7.287	−4.636*	−4.807
26 Picrodendrin M	**−9.305**	**−9.304**	**−9.305**	**−9.537**
27 Picrodendrin O	**−9.488**	**−8.394**	**−6.921**	**−7.004**
28 Picrodendrin P	**−7.572**	**−7.995**	**−4.636***	**−5.701**
29 Picrodendrin Q	−10.442	−10.128	−10.630	−10.504
30 Picrodendrin T	−7.616	−7.465	−6.830	−6.778

6: 14-acetoxy-3-oxofloridanolide; **7**: 13-acetoxy-14-(*n*-butyryloxy) floridanolide; **8**: 3β,14-dihydroxy-10-deoxyfloridanolide; **9**: 3β-acetoxy-14-*n*-butyryloxy-10-deoxyfloridanolide; **10**: 7-deoxy-7-oxodunnianin; **12**: 14-hydroxy-3-oxofloridanolide, *ortho*-lactone.
Experimental values marked by asterisks were obtained as explained in the methods section.
Values for compounds included in the *test set* are printed in boldface.

selectivity toward the insect receptor. The experimental binding affinity data for 13 *seco*-prezizaane type as well as 17 picrotoxane and picrodendrane-type terpenoids from our previous studies[7,9] (Table 1, compare structure diagram) were used to investigate quantitative structure–activity relationships (QSAR) by constructing binding site models utilizing the quasi-atomistic pseudoreceptor modeling approach of the program *Quasar*.[10,11]

The *Quasar* approach[10] is based on the construction of an envelope of virtual particles (pseudo-atoms) that represent the surface of a putative binding site. Each of these particles can adopt different physicochemical properties such as hydrogen bond donating or accepting capacity, electrostatic or hydrophobic interactions (full list of particle properties see Table 2). At the same time, induced fit of the receptor to the different compounds is taken into account by allowing the mean envelope of particles to adapt its shape to the individual compounds. Six different induced fit modes (linear, field-energy minimized, steric, electrostatic, lipophilic, hydrogen-bonding) can be modeled simultaneously. A genetic algorithm is used to find combinations of particle properties, which—in combination with the chosen induced fit mode—best reproduce the experimental binding energy (ΔG^0) derived from the biological data. The genetic algorithm produces a population of models whose properties are averaged and represent the final model. Construction of a *Quasar* model is carried out with a subset of the compounds, the training set, which should contain a representative spread of the total data set with respect to biological activity and chemical structure. Binding energies for another subset (test set), not used in the model building process, are then calculated in order to assess the predictive power (i.e., biological relevance) of the models. To further decrease the probability of chance correlations, scramble tests are performed with each model, where the biological data are randomly assigned to the molecules. Optimally, a scramble test should not lead to a relevant correlation between the predicted and scrambled biological data in order to assure that a substantial structure–activity correlation for the unscrambled data was not obtained by chance.

A validated *Quasar* model thus contains information on structure–activity relationships and can be used to predict the activity of new candidates. At the same time, it can also give insight into the physicochemical properties of the binding site within a biological target of unknown 3D structure.

Table 2. Analysis of particle distribution in final averaged models for the housefly (top) and rat receptor (bottom) binding site (number of individual models 200, total number of particles in both models: 201)

	Sum [1-6]	VL0 Hyd	VL1 Sb+	VL2 Sb−	VL3 Don	VL4 Acc	VL5 Hy+	VL6 Hy−
Housefly								
Min	68	113	5	6	5	6	21	7
Max	68	133	13	12	16	15	38	22
Ave	78.9	122.1	8.4	8.5	9.4	9.8	29.8	13.0
Ave%	39.3	60.7	4.2	4.2	4.7	4.9	14.8	6.5
Rat								
Min	81	101	9	5	7	2	19	15
Max	100	120	18	12	17	14	34	31
Ave	91.5	109.5	13.8	9.2	10.3	6.9	27.2	24.0
Ave%	45.5	54.5	6.9	4.6	5.1	3.4	13.5	11.9

VL0 Hyd = hydrophobic, neutral: GREY; VL1 Sb+ = salt bridge, positive: RED; VL2 Sb− = salt bridge, negative: BLUE; VL3 Don = hydrogen bond donor: GREEN; VL4 Acc = hydrogen bond acceptor: YELLOW; VL5 Hy+ = hydrophobic, positive: YELLOW BROWN; VL6 Hy− = hydrophobic, negative: RED BROWN; [VL7 (Flp = H-bond flip/flop), VL8 (Slv = solvent) and VL9 (Voi = void, no property) were not present in either model].

2. Results and discussion

Recently, we reported on a 3D-QSAR study for *seco*-prezizaanes and picrotoxanes/picrodendranes and their binding affinity toward the housefly GABA receptor using the CoMFA method.[7] The resulting QSAR indicated that the hypothesis concerning a common biophore and binding mode of these different types of terpenoids previously suggested on the basis of qualitative structure–activity considerations[8] was plausible. Based on the same alignment of the compounds (see Fig. 1) and binding data from our previous communications[7,9] models of the convulsant binding sites at both the housefly (*Musca domestica*) and the rat (*Rattus norvegicus*) GABA receptor were generated using *Quasar*, v. 4.0.[10,11]

2.1. Receptor surface model for the binding site at housefly GABA receptors

The data set under investigation ($n = 30$) was split into a variety of training ($n = 22$) and test sets ($n = 8$) (see structure diagram, for biological data see Table 1). Each combination was subjected to 5000 evolution steps applying the settings reported in the computational methods section. The model family presented below (Figs. 2 and 3) was the best obtained with respect to test set prediction. It consists of 200 individual models with 201 virtual particles whose property distribution is reported in Table 2. The induced fit model applied in all 200 final models is based on steric field interactions. The classical squared correlation coefficient for the training set r^2 is 0.91, the cross validated (leave 1/3 out) squared correlation coefficient for internal prediction q^2 is 0.90, and the squared correlation coefficient for the test set prediction p^2 is 0.69 with maximum and minimum values of 0.29 and 0.88, respectively (see Fig. 3A, predicted binding data see Table 1). Three independent scramble tests were performed under the same conditions, none of which yielded any relevant test set predictions (p^2 value negative in each case).

The final averaged model is depicted in Figure 2A. The hypothetical binding site possesses two major areas where polar/electrostatic interactions would take place. One comprises four salt-bridge acceptors (Sb^+ red, large spheres) and a hydrogen bond donor site (green, large spheres). This region is in the vicinity of the lactone carbonyl and ring oxygens of most of the compounds (corresponding to region A/B in Fig. 1). The second major polar region consists of five salt-bridge donors (Sb^- blue, large spheres) flanked by hydrogen bond acceptor sites (yellow, large spheres), which form a rel-

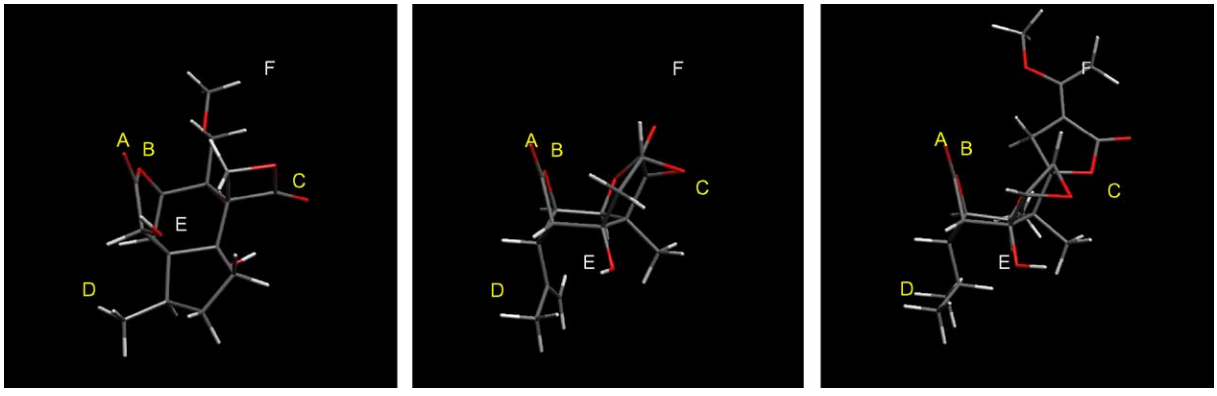

Figure 1. Molecular models of veranisatin A (**2**), picrotoxinin (**14**), and picrodendrin Q (**29**) aligned according to the pharmacophore hypothesis.[7,8] Molecule parts used for alignment are marked with yellow letters, white letters indicate further regions whose interactions with the pseudoreceptor models are discussed in the text.

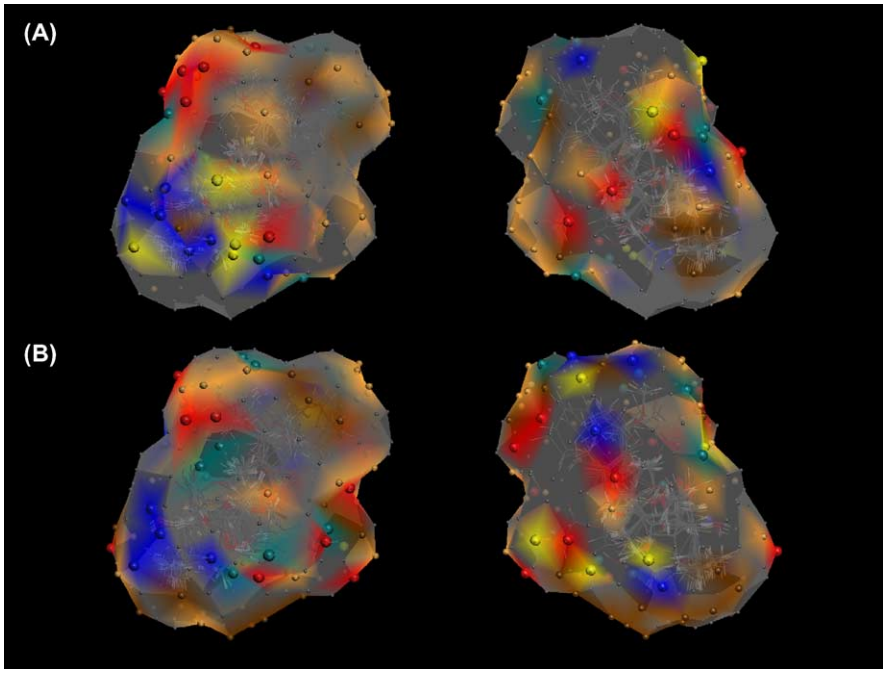

Figure 2. Pseudoreceptor models for the housefly (A) and the rat (B) binding site at GABA receptor-coupled chloride channels, viewed from two different angles ('front' and 'rear'). An overlay of all 30 compounds under study is shown in the same orientation as in Figure 1. Receptor particles: blue: salt bridge negative, SB−; red: salt bridge positive, SB+, yellow: hydrogen bond acceptor, Acc; green: hydrogen bond donor (Don); grey (small spheres): hydrophobic, neutral; yellow-brown (small spheres): hydrophobic positive (Hy−); red-brown (small spheres): hydrophobic, negative (Hy−).

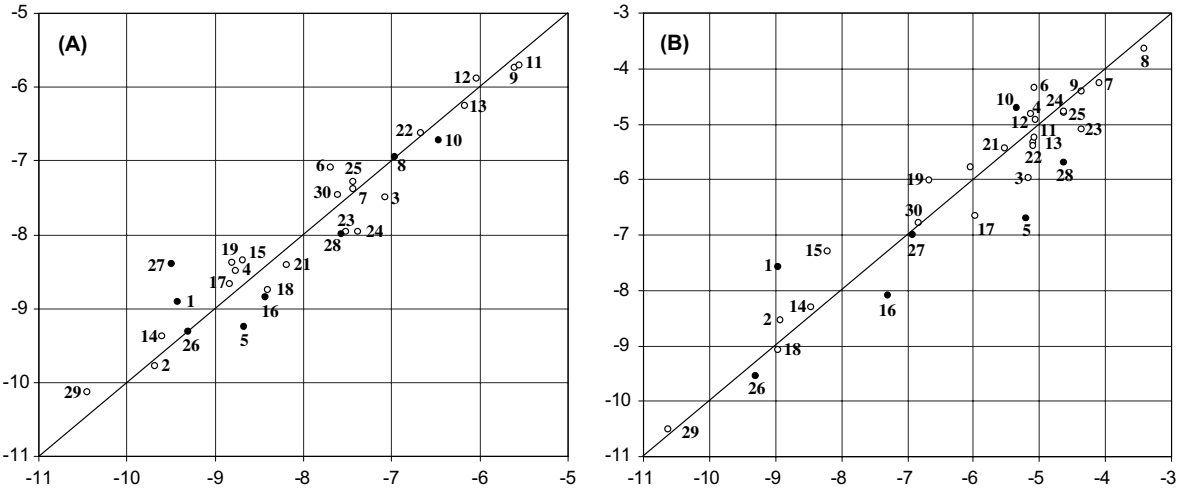

Figure 3. Plots of predicted versus measured binding energies (ΔG^0) toward the fly (A) and the rat (B) binding site models. Compounds of the training set open circles, those of the test set as black dots.

atively large area where hydrogen bonds/salt bridges can be formed with the protons on OH groups in the vicinity of positions marked with E in Figure 1. Adjacent to the mentioned areas of polar interactions, a relatively large region of hydrophobic interactions surrounding the lipophilic parts in area D, that is around the methylcyclopentane part of the *seco*-prezizaanes and the isoprop(en)yl residue of the picrotoxanes/picrodendranes, respectively, as well as the adjacent lower regions of the lactone ring, is observed. An additional hydrophobic pocket can accommodate the picrodendins' spiro-γ-lactone moiety (region F in Fig. 1). It is noteworthy in comparison with the model for the rat binding site (see below) that the region designated 'C' in Figure 1 does not show any major polar interactions.

2.2. Receptor surface model for the binding site at rat $GABA_A$ receptors

In order to identify differences between the insect and the mammalian receptor, an attempt was made to model the binding site in rat receptors using essentially the same conditions as applied in the housefly model. It must be mentioned that the biological data in this case show a rather conspicuous difference to those obtained

with the insect preparation. Active compounds are in most cases highly active while the number of intermediately active derivatives is small and a relatively large number of compounds only allowed measurement of a 'cut off' activity value, that is the activity was too low to measure an IC_{50} value directly. In these cases, binding data were estimated by extrapolation of a linear relationship between $\log(IC_{50})$ and the percent inhibition data obtained at 10 μM concentration for such compounds where both values were available (see methods section). These values are marked by an asterisk in Table 2. One of the test set compounds of the housefly model, compound **8**, which did not show any measurable affinity to the rat receptor was in this case used as the least active member of the *training* set. A *Quasar* model was obtained with the otherwise identical training- and test set with $r^2 = 0.91$, $q^2 = 0.90$ ($n = 23$) and $p^2 = 0.62$ (min. = 0.09, max. = 0.87; $n = 7$), see Figures 2B and 3B, predicted binding data see Table 1. As above, scramble tests confirmed the sensitivity of the model to the biological data. The statistical quality is somewhat inferior to the housefly model, which may, however, be explained by the use of estimated ΔG^0 values in many cases.

The final averaged model is relatively similar to the one described above (85 of the 201 particles = 42% show identical properties with those of the housefly model). Overall, the surface of the rat binding site appears to be slightly more polar (see particle property distribution in Table 2). Consistently, an electrostatic induced fit mode was used by all models. Many of the areas identified as important for binding at the insect model appear in a similar way also in the rat model, yet with slight differences in size or position, which would be in accordance with the expected similarity of the real binding sites where relatively few changes in amino acid sequence should have led to the dramatic changes in binding affinity observed for some of the compounds.

Thus, the rat receptor also shows the above-mentioned regions of polar interaction with molecule regions A/B and E as well as the nonpolar surface area corresponding to lipophilic molecule region D (compare Fig. 2A and B, left side). The 'rear part' is somewhat more polar in comparison with the insect model (compare Fig. 2A and B, right).

2.3. Differences between the rat and housefly receptor-surface models and implications with respect to insect selectivity

Figure 4 shows the structures of veranisatin A **2** (toxic to both, mammals and insects) and pseudoanisatin **4** (toxic only to insects) within the two binding site models. A noteworthy difference between the insect and rat receptor surrogates is observed in the region marked with arrows, where an SB+ (positively charged particle acting through electrostatic interaction) and a hydrogen bond donor site are found in the rat receptor instead of hydrophobic particles in the housefly model. This area can interact with the oxygen of the β-lactone ring in anisatin-type compounds or the corresponding epoxy groups in many picrotoxanes/picrodendranes (region C in Fig. 1). This fact is illustrated clearly in the structure of **2** bound to the rat receptor model (Fig. 4B, bottom), where a marked shift of the SB+ particle toward the β-lactone ring oxygen is observed in comparison with the corresponding model of **4** (Fig. 4A, bottom). One per-

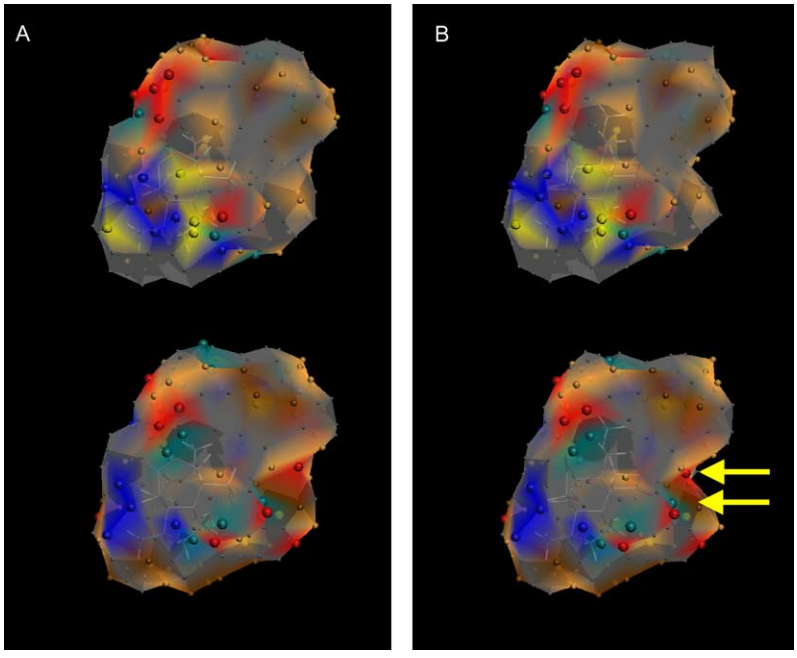

Figure 4. Pseudoanisatin (**4**, insect-selective; A) and veranisatin A (**2**, nonselective, B) shown inside the fly (top) and rat (bottom) binding site models. Note the interaction of the β-lactone ring oxygen of **2** with the SB+ and Don particles on the right side of the rat binding site (arrows). Especially the SB+ particle is moved toward the lactone oxygen as compared to compound **4**.

tinent reason for the differential binding affinity of the insect-selective compounds apparently lies in their inability to engage in interactions with this part of the mammalian receptor while on the other hand, high affinity binding to the insect receptor does not require this interaction.

Quasar allows an analysis of a particular compound's interactions with the receptor surface in terms of functional group contributions to binding energy. This analysis yields for each functional group a numerical value (kcal/mol) expressing its contribution to the overall predicted binding energy, ΔG^0. These interactions can then be color-coded into the 3D-structure model allowing direct visual interpretation of the binding data in terms of structural contributions. Moreover, for each functional group the different binding terms (van der Waals, electrostatic, hydrogen bonding) contributing to its total interaction are obtained. Figure 5 shows the results of the functional group analysis for veranisatin A **2** and pseudoanisatin **4**, which are also summarized in numerical form in Table 3. The selectivity of **4** can thereby be rationalized on the basis of few major structural determinants. The C-7 oxo group shows a strong negative value (enhancement of binding) to the insect binding site while its value at the rat binding site is even slightly positive indicating a detrimental effect on affinity. As deduced from the *Quasar* output, this follows from an enhancement of electrostatic and hydrogen bonding interactions of this group in the insect model. The ε-lactone carbonyl group shows a detrimental effect at both receptors, which is, however,

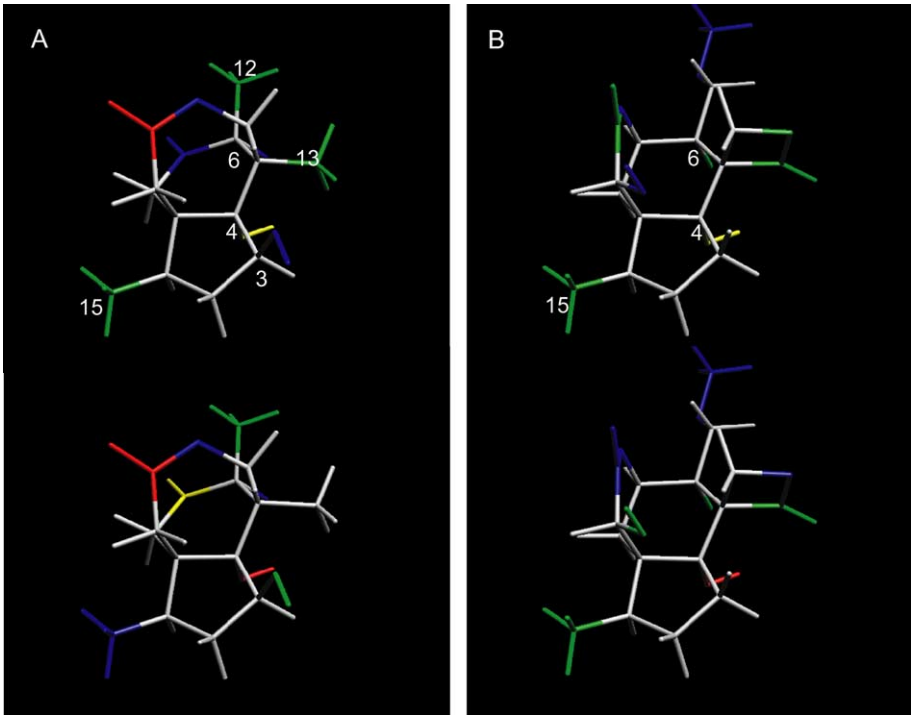

Figure 5. Results of the functional group analysis for compounds **4** (A) and **2** (B) in the fly (top) and rat (bottom) pseudoreceptor models. Group contributions to binding energy (compare Table 3) are color-coded by: blue = good; green = fair; white = neutral; yellow = poor; red = bad.

Table 3. Results of the functional group analysis for pseudoanisatin **4** and veranisatin A **2** at the housefly and rat pseudoreceptor models

Pseudoanisatin (**4**)				Veranisatin A (**2**)			
	Fly	Rat	Diff		Fly	Rat	Diff
C═O (ε-lactone)	0.9	2.0	**−1.1**	C═O (δ-lactone)	−0.6	−1.4	0.8
O (ε-lactone)	−0.9	−2.2	1.3	O (δ-lactone)	−0.7	−0.6	−0.1
C═O (ketone)	−1.2	0.3	**−1.5**	C═O (β-lactone)	−0.7	−0.1	−0.6
OH at C-3	−1.6	−0.5	**−1.1**	O (β-lactone)	−0.2	−1.2	1.0
C-4-OH	0.3	1.0	−0.7	C-4-OH	0.1	1.0	−0.9
C-6-OH	−0.7	−1.0	0.3	C-6-OH	−0.5	−0.2	−0.3
CH_3-12	−1.0	−0.8	−0.2	C-10-OH	−1.4	−0.7	−0.7
CH_3-13	−0.4	0.0	−0.4	OCH_3	−2.7	−2.6	−0.1
CH_3-15	−1.3	−1.1	−0.2	CH_3-15	−1.5	−1.3	−0.2
Residual	−2.6	−2.5	−0.1	Residual	−1.6	−1.4	−0.2
Total	−8.5	−4.8	−3.7	Total	−9.8	−8.5	−1.3

Contributions of the various functional groups to the total predicted binding energies in kcal/mol; residual: part of binding energy not explained by the mentioned functional group interactions. Compare Figure 5.

much stronger at the rat model leading to poorer binding to the mammalian receptor. Moreover, the contribution of the C-3β-OH group is significantly stronger toward the insect binding site, caused by increased hydrogen bond formation. In parviflorolide **5**, similarly selective toward insect receptors, the same applies to the C-10β-OH group (data not shown), which in the 3D structure occupies a similar position. The differences in group contributions between the two models (ΔG (fly) − ΔG (rat), see Table 3) illustrate these groups' importance.

Comparison of the data for veranisatin A **2**, on the other hand, shows that the difference in group contributions between the two models is much smaller, reflecting the absence of selectivity (see Table 3). A major difference is observed for the ring oxygen of the β-lactone moiety, which contributes strongly to binding at the rat receptor (main determinant: electrostatic interaction) but shows almost no contribution to the insect model. This oxygen's most prominent interaction in the rat binding site is with the above-mentioned SB+ and Don-particles (marked by arrows in Fig. 4) while the insect receptor does not show this additional anchor point. Thus, an insect-selective compound should not possess an oxygen (or other electronegative function capable of donating electron density into a salt bridge or, possibly, of accepting a hydrogen bond) in this area. At the same time it may be concluded that a 7,11-δ-lactone structure should not be present since the carbonyl group of this element confers a much stronger binding contribution (due to improved H bonding) toward the rat than toward the insect receptor surface model.

The results of this study provide valuable information with respect to further lead optimization toward insect-selective GABA antagonists and give new insight into the structural differences of the binding sites for terpenoid convulsants at insect and mammalian GABA receptor-coupled chloride channels.

Attempts to design *seco*-prezizaane derivatives with even higher selectivity on the basis of the results of the current report are in progress. Prediction of binding energies for a variety of derivatives of **4** and **5** allowed us to devise structures with $\delta\Delta G^0$ (rat-fly) of 5–6 kcal mol^{-1}, corresponding to a predicted ratio of IC_{50} values in the range of 5000–50,000. The evaluation of these derivatives is under way and will be addressed in a subsequent report.

Moreover, we are conducting studies to include also other classes of convulsants/insecticides into our QSAR.

3. Methods

3.1. Biological data

The binding data for all compounds were extracted from our previous reports.[7,9]

IC_{50} values for displacement of [^{3}H]EBOB were converted into binding energies at $T = 298$ K following the assumption that $\Delta G^0 = -RT \ln(IC_{50}(M))$. The data for each compound are reported in Table 1. In cases where activity was too low to permit direct measurement of an IC_{50} value, the data were estimated on the basis of their % inhibition at 10 μM concentration (%10 μM) by the following method. The %10 μM values were plotted against $-\log(IC_{50})$ for such compounds where both values were available. In order to avoid errors caused by non-linearity at very high %10 μM values, only such compounds where %10 μM < 99% were included. Linear regression analysis for the rat data (six compounds ranging between %10 μM = 92 to 52.5 and $-\log(IC_{50})$ between 6.2 and 5.0) yielded a squared correlation coefficient $r^2 = 0.993$. In case of the housefly data, for six compounds (all of the *seco*-prezizaane series) ranging between %10 μM = 97.7 and 42.7 and $-\log(IC_{50})$ between 6.4 and 5.1, r^2 was 0.943. The linear regression equations thus obtained were then used to calculate $\log(IC_{50})$ values for those compounds whose IC_{50} values could not be determined directly, that is where only %10 μM values were available. Values obtained in this way are marked with an asterisk in Table 1.

3.2. Computational methods

All computations were performed on a 2.4 GHz Pentium 4 personal computer.

3.3. Molecular modeling

Initial molecular models of each compound were generated as described previously.[7] Conformational searches were performed for all compounds using MOE.[12] For each compound, the lowest energy conformer as found by a stochastic conformational search (MMFF94 force field) was submitted to energy minimization to an RMS gradient <0.1 kcal mol^{-1} Å^{-1} using the semiempirical AM1 hamiltonian[13] (HYPERCHEM v. 7.0).[14] Partial atomic charges were derived from the AM1 wavefunction. Alignment of the compounds was performed in essentially the same way as reported previously.[7,8]

3.4. Receptor surface modeling and QSAR analysis

The program *Quasar*, v. 4.0,[10,11] graphic version for PC (Win *Quasar*) was used for the receptor surface modeling and visualization as depicted in Figures 1–5.

The pseudoreceptor models were generated using the training/test set splits reported in Table 1. Module 'Prepare': All compounds were included as MOL2-files. No internal energy corrections were applied. Module 'Envelope': For each compound, all six possible induced fit models were taken into account in the generation of individual envelopes. Module *Quasar*: The option 'diffuse properties' allowing a diffusion of each particle's properties over the adjacent surface region was turned on, using the preset parameters. Two hundred randomly

generated individual models were submitted to the genetic algorithm, allowing for dynamic change of mutation rate. The termination criterion $q^2 = 0.90$ was in both cases reached after <5000 crossovers.

All output data related to the final presented models can be obtained from the corresponding author on request (electronic form).

Acknowledgements

The authors thank Dr. Angelo Vedani, Biographics Laboratory 3R, Basel, Switzerland, for valuable discussions.

References and notes

1. Bormann, J. *Trends Pharmacol. Sci.* **2000**, *21*, 16.
2. Rabow, L. E.; Russek, S. J.; Farb, D. H. *Synapse* **1995**, *21*, 189.
3. Hosie, A. M.; Aronstein, K.; Sattelle, D. B.; ffrench-Constant, R. H. *Trends Neurosci.* **1997**, *20*, 578.
4. Mezler, M.; Muller, T.; Raming, K. *Eur. J. Neurosci.* **2001**, *13*, 477.
5. Gant, D. B.; Chalmers, A. E.; Wolff, M. A.; Hoffman, H. B.; Bushey, D. F. *Rev. Toxicol.* **1998**, *2*, 147.
6. Schmidt, T. J.; Schmidt, H. M.; Müller, E.; Peters, W.; Fronczek, F. R.; Truesdale, A.; Fischer, N. H. *J. Nat. Prod.* **1997**, *60*, 783.
7. Kuriyama, T.; Schmidt, T. J.; Okuyama, E.; Ozoe, Y. *Bioorg. Med. Chem.* **2002**, *10*, 1873.
8. Schmidt, T. J.; Okuyama, E.; Fronczek, F. R. *Bioorg. Med. Chem.* **1999**, *7*, 2857.
9. Ozoe, Y.; Akamatsu, M.; Higata, T.; Ikeda, I.; Mochida, K.; Koike, K.; Ohmoto, T.; Nikaido, T. *Bioorg. Med. Chem.* **1998**, *6*, 481.
10. Vedani, A.; Dobler, M. *J. Med. Chem.* **2002**, *45*, 2139.
11. *Quasar*-Manual, http://www.biograf.ch.
12. MOE (The Molecular Operations Environment) V. 2003.02, available from Chemical Computing Group, 1010 Sherbrooke St. West, Suite 910, Montreal, Quebec, Canada H3A2R7. http://www.chemcomp.com.
13. Dewar, M. J. S.; Thiel, W. *J. Am. Chem. Soc.* **1977**, *99*, 4499.
14. HYPERCHEM v. 7.0, is a product of Hypercube. http://www.hyper.com.